Physics Letters B 805 (2020) 135454

Contents lists available at ScienceDirect

Physics Letters B

www.elsevier.com/locate/physletb

Measurement of the cross section for hard exclusive π^0 muoproduction on the proton

The COMPASS Collaboration

ARTICLE INFO

Article history:
Received 29 March 2019
Received in revised form 22 April 2020
Accepted 22 April 2020
Available online 5 May 2020
Editor: M. Doser

Keywords:
Quantum chromodynamics
Muoproduction
Hard exclusive meson production
Generalised Parton Distributions
COMPASS

ABSTRACT

We report on a measurement of hard exclusive π^0 muoproduction on the proton by COMPASS using 160 GeV/c polarised μ^+ and μ^- beams of the CERN SPS impinging on a liquid hydrogen target. From the average of the measured μ^+ and μ^- cross sections, the virtual-photon proton cross section is determined as a function of the squared four-momentum transfer between initial and final proton in the range $0.08\,(\mathrm{GeV}/c)^2 < |t| < 0.64\,(\mathrm{GeV}/c)^2$. The average kinematics of the measurement are $\langle Q^2 \rangle = 2.0\ (\mathrm{GeV}/c)^2$, $\langle \nu \rangle = 12.8$ GeV, $\langle x_{Bj} \rangle = 0.093$ and $\langle -t \rangle = 0.256\ (\mathrm{GeV}/c)^2$. Fitting the azimuthal dependence reveals a combined contribution by transversely and longitudinally polarised photons of $(8.2 \pm 0.9_{\mathrm{stat}}{}^{+\ 1.2}_{-\ 1.2}|_{\mathrm{sys}})\ \mathrm{nb}/(\mathrm{GeV}/c)^2$, as well as transverse-transverse and longitudinal-transverse interference contributions of $(-6.1 \pm 1.3_{\mathrm{stat}}{}^{+\ 0.7}_{-\ 0.7}|_{\mathrm{sys}})\ \mathrm{nb}/(\mathrm{GeV}/c)^2$ and $(1.5 \pm 0.5_{\mathrm{stat}}{}^{+\ 0.3}_{-\ 0.2}|_{\mathrm{sys}})\ \mathrm{nb}/(\mathrm{GeV}/c)^2$, respectively. Our results provide important input for modelling Generalised Parton Distributions. In the context of the phenomenological Goloskokov-Kroll model, the statistically significant transverse-transverse interference contribution constitutes clear experimental evidence for the chiral-odd GPD $\overline{E}_T$.

1. Introduction

Measurements of pseudoscalar mesons produced in hard exclusive lepton-nucleon scattering provide important data for phenomenological parameterisations of Generalised Parton Distributions (GPDs) [1–5]. In the past two decades, GPDs have shown to be a very rich and useful construct for both experiment and theory as their determination allows for a detailed description of the parton structure of the nucleon. In particular, GPDs correlate transverse spatial positions and longitudinal momentum fractions of the partons in the nucleon. They embed parton distribution functions and nucleon form factors, and they give access to energy-momentum-tensor form factors. For each quark flavour, there exist four parton-helicity-conserving (chiral-even) GPDs, denoted H, $\tilde{H}$, E, and $\tilde{E}$, and four parton-helicity-flip (chiral-odd) GPDs, denoted H_T, $\tilde{H}_T$, E_T, and $\tilde{E}_T$. While hard production of vector mesons is sensitive primarily to the GPDs H and E, the production of pseudoscalar mesons by longitudinally polarised virtual photons is sensitive to $\tilde{H}$ and $\tilde{E}$ in the leading-twist description.

Contributions from transversely polarised virtual photons to the production of spin-0 mesons are expected to be suppressed in the production amplitude by $1/Q$ [6], where Q^2 is the virtuality of the photon γ^* that is exchanged between muon and proton. However, experimental data on exclusive π^+ production from HERMES [7] and on exclusive π^0 production from JLab CLAS [8–11] and Hall A [12–14] suggest that such contributions are substantial. In the GPD formalism such contributions are possible if a quark helicity-flip GPD couples to a twist-3 meson wave function [15,16]. In the framework of the phenomenological model of Ref. [15], pseudoscalar-meson production is described by the GPDs $\tilde{H}$, $\tilde{E}$, H_T and $\overline{E}_T = 2\tilde{H}_T + E_T$. Different sensitivities to these GPDs are expected when comparing π^+ vs. π^0 production. When taking into account the relative signs and sizes of these GPDs for u and d quarks, the different quark flavour contents of these mesons lead to different predictions for the $|t|$-dependence of the cross section, especially at small values of $|t|$. Here, t is the square of the four-momentum transfer between initial and final nucleon. The production of π^+ mesons is dominated by the contributions from longitudinally polarised virtual photons, of which a major part originates from pion-pole exchange that is the main contributor to $\tilde{E}$. Also the contributions from $\tilde{H}$ and H_T are significant, and there is a strong cancellation between the contributions from $\overline{E}_T$ for u and d quarks. On the contrary, in the case of π^0 production there is no pion-pole exchange, the contributions from $\tilde{H}$ and H_T are small and a large contribution from transversely polarised photons is generated mainly by $\overline{E}_T$.

These differences between π^+ and π^0 production are experimentally supported. While for π^+ production a fast decrease of the cross section with increasing $|t|$ is predicted by theoretical models and confirmed by the experimental results from HERMES [7], for π^0 production a dip is expected as $|t| \to 0$ [15] and confirmed by results in the JLab kinematic domain [9,10,13]. Constraints for modelling the poorly known GPD $\overline{E}_T$ were obtained in a lattice-QCD study [17] of its moments. The COMPASS results on

https://doi.org/10.1016/j.physletb.2020.135454

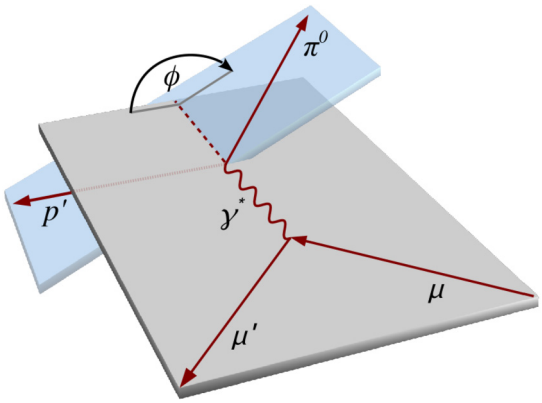

Fig. 1. Definition of ϕ, the azimuthal angle between the lepton-scattering and π^0-production planes.

exclusive π^0 production in muon-proton scattering presented in this Letter provide new input for modelling this GPD and chiral-odd ('transversity') GPDs in general.

2. Formalism

The reduced cross section for hard exclusive meson production by scattering a polarised lepton beam off an unpolarised proton target reads:

$$\frac{\mathrm{d}^2\sigma^{\leftrightarrows}_{\gamma^* p}}{\mathrm{d}t\mathrm{d}\phi} = \frac{1}{2\pi}\Big[\frac{\mathrm{d}\sigma_T}{\mathrm{d}t} + \epsilon\frac{\mathrm{d}\sigma_L}{\mathrm{d}t} + \epsilon\cos(2\phi)\frac{\mathrm{d}\sigma_{TT}}{\mathrm{d}t} + \sqrt{2\epsilon(1+\epsilon)}\cos\phi\frac{\mathrm{d}\sigma_{LT}}{\mathrm{d}t} \mp |P_l|\sqrt{2\epsilon(1-\epsilon)}\sin\phi\frac{\mathrm{d}\sigma'_{LT}}{\mathrm{d}t}\Big], \tag{1}$$

where the sign $\mp$ of the lepton beam polarisation P_l corresponds to negative and positive helicity of the incoming lepton, respectively, denoted by $\leftrightarrows$. The conversion from the lepton-nucleon cross section to the virtual-photon nucleon cross section, using the one-photon-exchange approximation, is explained in Sect. 5. The contribution to the cross section from transversely (longitudinally) polarised virtual photons is denoted by σ_T (σ_L). The symbols σ_{LT}, σ'_{LT} and σ_{TT} denote contributions from the interference between longitudinally and transversely polarised virtual photons, and between transversely polarised virtual photons of opposite helicity. The factor

$$\epsilon = \frac{1 - y - \frac{y^2\gamma^2}{4}}{1 - y + \frac{y^2}{2} + \frac{y^2\gamma^2}{4}} \tag{2}$$

is the virtual-photon polarisation parameter and ϕ is the azimuthal angle between the lepton scattering plane and the hadron production plane, see Fig. 1. Here, $Q^2 = -(k_\mu - k_{\mu'})^2$ is the photon virtuality, $\nu = (k^0_\mu - k^0_{\mu'})$ the energy of the virtual photon in the target rest frame, $y = \nu/k^0_\mu$ and $\gamma^2 = Q^2/\nu^2$, where k_μ and $k_{\mu'}$ denote the four-momenta of the incoming and the scattered muon in the target rest frame, respectively.

The spin-independent cross section can be obtained by averaging the two spin-dependent cross sections,

$$\frac{\mathrm{d}^2\sigma_{\gamma^* p}}{\mathrm{d}t\mathrm{d}\phi} = \frac{1}{2}\Big(\frac{\mathrm{d}^2\sigma^{\leftarrow}_{\gamma^* p}}{\mathrm{d}t\mathrm{d}\phi} + \frac{\mathrm{d}^2\sigma^{\rightarrow}_{\gamma^* p}}{\mathrm{d}t\mathrm{d}\phi}\Big). \tag{3}$$

When forming this average, the last term in Eq. (1) cancels if the magnitude $|P_l|$ of the beam polarisation is the same for measurements with μ^+ and μ^- beam, so that

$$\frac{\mathrm{d}^2\sigma_{\gamma^* p}}{\mathrm{d}t\mathrm{d}\phi} = \frac{1}{2\pi}\Big[\frac{\mathrm{d}\sigma_T}{\mathrm{d}t} + \epsilon\frac{\mathrm{d}\sigma_L}{\mathrm{d}t} + \epsilon\cos(2\phi)\frac{\mathrm{d}\sigma_{TT}}{\mathrm{d}t} + \sqrt{2\epsilon(1+\epsilon)}\cos(\phi)\frac{\mathrm{d}\sigma_{LT}}{\mathrm{d}t}\Big]. \tag{4}$$

The individual contributions appearing in Eq. (4) are related to convolutions of GPDs and meson wave functions with individual hard scattering amplitudes, see Refs. [10,15]:

$$\frac{\mathrm{d}\sigma_T}{\mathrm{d}t} \propto \Big[(1-\xi^2)|\langle H_T\rangle|^2 - \frac{t'}{8M^2}|\langle\overline{E}_T\rangle|^2\Big], \tag{5}$$

$$\frac{\mathrm{d}\sigma_L}{\mathrm{d}t} \propto \Big[(1-\xi^2)|\langle\tilde{H}\rangle|^2 - 2\xi^2 Re\Big[\langle\tilde{H}\rangle^*\langle\tilde{E}\rangle\Big] - \frac{t'}{4M^2}\xi^2|\langle\tilde{E}\rangle|^2\Big], \tag{6}$$

$$\frac{\mathrm{d}\sigma_{TT}}{\mathrm{d}t} \propto t'|\langle\overline{E}_T\rangle|^2, \tag{7}$$

$$\frac{\mathrm{d}\sigma_{LT}}{\mathrm{d}t} \propto \xi\sqrt{1-\xi^2}\sqrt{-t'}Re\Big[\langle H_T\rangle^*\langle\tilde{E}\rangle\Big]. \tag{8}$$

Here, the aforementioned convolutions are denoted by triangular brackets, $t' = t - t_{min}$ with $|t_{min}|$ being the kinematically smallest possible value of $|t|$, and M is the mass of the proton. The quantity ξ is equal to one half of the longitudinal momentum fraction transferred between the initial and final proton and can be approximated at COMPASS kinematics as

$$\xi \approx \frac{x_{\mathrm{Bj}}}{2 - x_{\mathrm{Bj}}}, \tag{9}$$

where $x_{\mathrm{Bj}} = Q^2/(2M\nu)$.

3. Experimental set-up and data selection

The main component of the COMPASS set-up is the two-stage magnetic spectrometer. Each spectrometer stage comprises a dipole magnet complemented by a variety of tracking detectors, a muon filter for muon identification and an electromagnetic (ECal) as well as a hadron calorimeter. A detailed description of the set-up can be found in Refs. [18–20].

The data used for this analysis were collected using a 160 GeV/c muon beam within four weeks in 2012, during which the COMPASS spectrometer was complemented by a 2.5 m long liquid-hydrogen target surrounded by a time-of-flight (TOF) system, and a third electromagnetic calorimeter that was placed directly downstream of the target [20,21]. The TOF detector consisted of two cylinders mounted concentrically around the target, each made of 24 scintillating-counter slats with read-out at both ends of every slat. The read-out scheme allowed to measure the time-of-flight between two layers, determine the hit positions of a particle upon traversal through a layer and measure the energy loss in each layer. This allows us to determine polar angle and momentum of the particle.

In order to determine the spin-independent cross section through Eq. (3), data with μ^+ and μ^- beam were taken separately. The natural polarisation of the muon beam provided by the CERN SPS originates from the parity-violating decay in flight of the parent meson, which implies opposite polarisation for μ^+ and μ^- beams. Within regular time intervals during the measurement, charge and polarisation of the muon beam were swapped simultaneously. In order to equalize the spectrometer acceptance for the two beam charges, also the polarities of the two spectrometer magnet currents were changed accordingly. In total, a luminosity of 18.9 pb^{-1} was collected for the μ^+ beam with negative polarisation and 23.5 pb^{-1} for the μ^- beam with positive polarisation. The integrated beam flux was measured using a specific trigger

embedded in the standard COMPASS data taking based on a radioactive source [22] and is known with an uncertainty of 3%. For both beams, the absolute value of the average beam polarisation is about 0.8 with an uncertainty of about 0.04 [18,23].

For the analysis, only data taken with stable beam and spectrometer conditions are used. The selection of π^0 mesons is accomplished using their dominant two-photon decay. The threshold for the decay photon with lower energy is 300 MeV, while that for the photon with higher energy is 1 GeV for the most upstream calorimeter and 2 GeV for the calorimeter in the first stage of the spectrometer. The most downstream calorimeter is not used in this analysis as it contributes only very small statistics to the π^0 sample. At least two neutral clusters are required that had to be detected in any of the electromagnetic calorimeters above the respective threshold, in conjunction with an interaction vertex reconstructed within the target using the incoming and outgoing muon tracks. The outgoing muon is identified by requiring that it has the same charge as the beam particle and traverses more than 15 radiation lengths. As neutral cluster we denote a reconstructed calorimeter cluster that is not associated to a charged track, thereby including any cluster in case of the most upstream calorimeter that had no tracking system in front.

For each interaction vertex and each combination of two neutral clusters, the kinematics of the recoil proton are predicted from the four-momentum balance of the analysed process, $\mu p \to \mu' p' \pi^0$, $\pi^0 \to \gamma\gamma$, by using the reconstructed spectrometer information, i.e. the vertex position, the momenta of the incoming and outgoing muons as well as the energy and position of the two clusters. The predicted properties of the recoil proton p' are compared to the properties of each track candidate as reconstructed by the TOF system. Note that the four-momentum of the recoil proton is determined by the target TOF system based on the assumption that the reconstructed track belongs to a proton.

The following exclusivity constraints are used to select events for the cross-section determination:

$$|\Delta\varphi| < 0.4\,\text{rad},$$
$$|\Delta p_T| < 0.3\,\text{GeV}/c,$$
$$|\Delta z| < 16\,\text{cm},$$
$$|M_X^2| < 0.3\,(\text{GeV}/c^2)^2.$$

Here, $\Delta\varphi$ is the difference between predicted and measured azimuthal angle of the recoil proton candidate; Δp_T is the difference between predicted and measured transverse momentum of the recoil proton candidate; Δz is the difference between predicted and measured hit position in the inner ring of the TOF system. The quantity p_T is defined in the target rest frame. The undetected mass is given by

$$M_X^2 = (k_\mu + p_p - k_{\mu'} - p_{p'} - p_{\gamma_1} - p_{\gamma_2})^2\,. \tag{10}$$

Here, the four-momenta are denoted by p_p and $p_{p'}$ for the target and recoil proton, respectively, and by p_{γ_1} and p_{γ_2} for the two produced photons. In addition a constraint on the invariant mass $M_{\gamma\gamma}$ is used:

$$0.1092 < M_{\gamma\gamma}/(\text{GeV}/c^2) < 0.1576\,.$$

In the case that more than one combination of vertex, cluster pair and recoil-track candidate exist that satisfy the aforementioned selection criteria for a given event, this event is excluded from the analysis.

Fig. 2 shows an example for the result of a comparison between predicted and measured kinematics of the recoil candidate, and Figs. 3 and 4 show correspondingly the distributions of undetected mass and two-photon mass. In these figures, the four

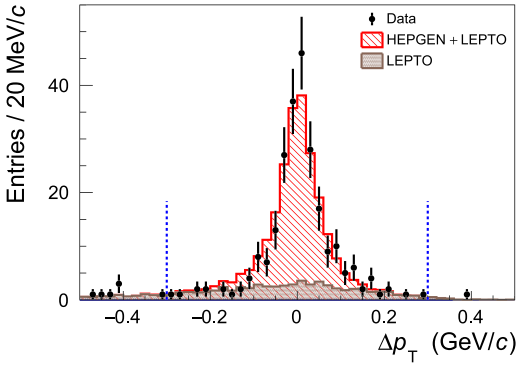

Fig. 2. Measured and simulated distribution of Δp_T of the recoil proton for the kinematic region described in the text. The vertical lines indicate the constraints applied for the selection of events. Error bars denote statistical uncertainties.

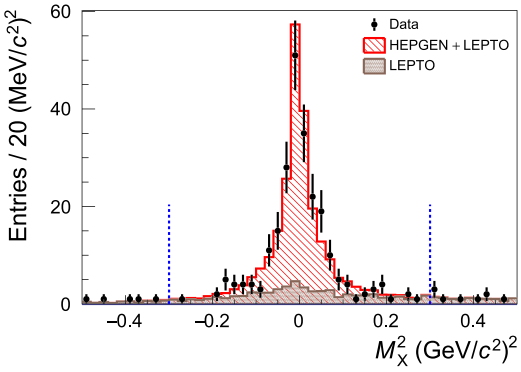

Fig. 3. Distribution of the undetected mass M_X^2. Otherwise as in Fig. 2.

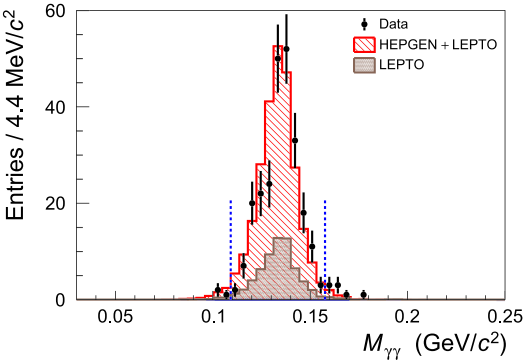

Fig. 4. Distribution of the invariant mass $M_{\gamma\gamma}$ of the two-photon system. Otherwise as in Fig. 2.

exclusivity constraints as well as the $|M_{\gamma\gamma}|$ constraint and single vertex/recoil-proton-candidate selection are applied. Additionally applied are constraints on the pull distributions of incoming and outgoing muon, the position of ECAL clusters and the ϕ-value of hits in the recoil-proton detector, as determined using the kinematic fit described below. Here, a pull is defined as ratio of the difference between the measured and the fitted value of a given quantity, and the standard deviation of this difference.

Note that the quantity presented in a given figure is not constrained and that every figure displays numeric values before the kinematic fit.

The Monte Carlo yields shown in these figures are denoted as HEPGEN and LEPTO. These generators are introduced in Sect. 4. The generated events from both generators are independently passed through a complete description of the COMPASS set-up [24], and

the resulting simulated data are treated in the same way as it is done for real data.

In order to enhance the purity of the selected data and to improve the precision of the particle kinematics at the interaction vertex, a kinematic fit for the exclusive reaction $\mu p \to \mu' p' \pi^0$ is performed, which requires a single π^0 to decay into the two photons selected as described above.

Together with the selection procedure given above, the requirements

$$0.08\,(\mathrm{GeV}/c)^2 < |t| < 0.64\,(\mathrm{GeV}/c)^2,$$
$$1\,(\mathrm{GeV}/c)^2 < Q^2 < 5\,(\mathrm{GeV}/c)^2,$$
$$8.5\,\mathrm{GeV} < \nu < 28\,\mathrm{GeV}$$

are used to obtain the events for the determination of the exclusive π^0 cross section as described in Sect. 5. The resulting minimum value of W is about $3.5\,\mathrm{GeV}/c^2$.

4. Estimation of the background contribution

In order to obtain a larger event sample for the study of the background, two reference samples are selected in the wider kinematic range $|t| > 0.08\,(\mathrm{GeV}/c)^2$, $Q^2 > 1\,(\mathrm{GeV}/c)^2$ and $y > 0.05$. These two samples are denoted as signal and background sample in this section. In contrast to the signal sample, the background sample contains only events with more than one combination of vertex, cluster pair and recoil-track candidate. Apart from the small peak at zero (see Fig. 5 bottom), it contains non-exclusive events. The purpose of the reference samples is explained in the following section.

The main background to exclusive π^0 muoproduction originates from non-exclusive deep-inelastic scattering processes. In such processes, low-energy hadrons are produced in addition to the π^0, which remain undetected in the apparatus. In order to estimate the background contribution, two Monte Carlo generators are employed.

First, the LEPTO 6.5.1 generator with the COMPASS tuning [25] is used to describe the non-exclusive fraction of events. Secondly, the HEPGEN++ π^0 generator, which is denoted HEPGEN in this paper, is used to model the kinematics of single π^0 muoproduction [26,27]. Note that events with the topology of exclusive π^0 production were removed from the LEPTO sample.

As there exists essentially no information on the cross section of exclusive π^0 production in the kinematic domain of COMPASS, the two reference samples described above are used to normalise the HEPGEN and LEPTO Monte Carlo yields. Using several variables, the kinematic information from beam and spectrometer measurements as well as that of the recoil-proton candidates are compared between experimental data and the two simulations in order to determine the best normalisation of each simulated data set relative to that of the experimental data. This comparison is done without applying the kinematic fit. As an example of such a comparison, the undetected mass is shown in Fig. 5. In addition to the measured data points, the HEPGEN simulation and the sum of the HEPGEN and LEPTO simulations are shown. In order to estimate the amount of non-exclusive background, the simulated data are scaled such that they describe the data for both reference samples. The scaling factor for the LEPTO Monte Carlo yield, which is denoted by $f^{\pm}$ for the two beam charges, will be used in Sect. 5 to normalise this simulation when correcting the data for background.

Using the scaling factors $f^{\pm}$, the fraction of non-exclusive background in the data is estimated to be $(29^{+\,2}_{-\,6}|_{\mathrm{sys}})\%$. Here, the uncertainty is estimated by comparing the scaling factors extracted for various variables and by using several extraction methods for the scaling factors. Details are given in Ref. [28]. Contributions of other background sources are found to be negligible. For example, the production of single ω mesons, where the ω decays into a π^0 and a photon that remains undetected, was found in Monte Carlo studies to contribute at the level of 1% [28].

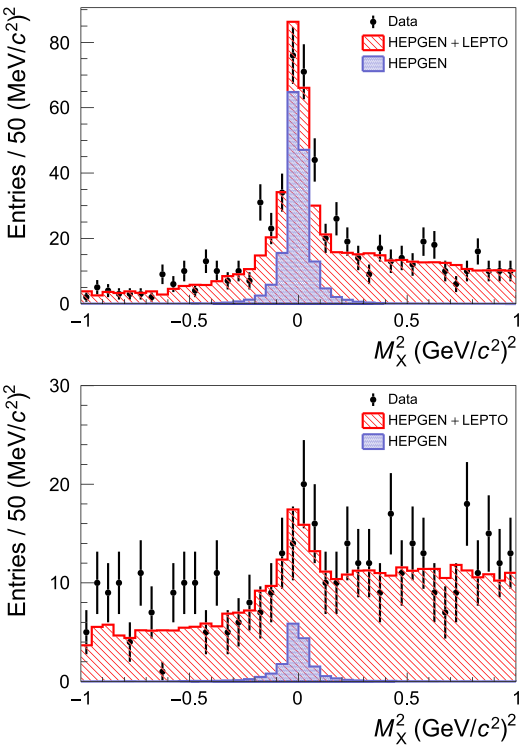

Fig. 5. Data used for the determination of the background contribution: Distributions of the undetected mass M_X^2 for the signal (top) and background (bottom) reference samples, which are selected in the extended kinematic range. Simulated data are also shown (see text). Error bars denote statistical uncertainties.

5. Determination of the cross section

The virtual-photon proton cross section is obtained from the measured muon-proton cross section using

$$\frac{\mathrm{d}^2\sigma}{\mathrm{d}|t|\mathrm{d}\phi} = \frac{1}{\Gamma(Q^2,\nu,E_\mu)}\,\frac{\mathrm{d}\sigma^{\mu p}}{\mathrm{d}Q^2\mathrm{d}\nu\mathrm{d}\phi\mathrm{d}|t|}, \tag{11}$$

where the transverse virtual-photon flux is given by

$$\Gamma(Q^2,\nu,E_\mu) = \frac{\alpha_{\mathrm{em}}(1-x_{\mathrm{Bj}})}{2\pi\,Q^2 y E_\mu}\left[y^2\left(1-\frac{2m_\mu^2}{Q^2}\right) + \frac{2}{1+Q^2/\nu^2}\left(1-y-\frac{Q^2}{4E_\mu^2}\right)\right]. \tag{12}$$

Here, α_{em} denotes the electromagnetic fine structure constant and $E_\mu = k_\mu^0$.

For the cross section determination, the HEPGEN Monte Carlo simulation described in Sect. 4 is used. The acceptance $a(\Delta\Omega_{klmn})$ is calculated in a four-dimensional grid as the number of reconstructed events divided by the number of generated events using 8 bins in ϕ, 5 in $|t|$, 4 in Q^2 and 4 in ν, including bin-to-bin event migration. The phase-space element is given by $\Delta\Omega_{klmn} = \Delta\phi_k \Delta|t|_l \Delta Q^2_m \Delta\nu_n$. The spacing of the grid is given in Table 1.

In each four-dimensional bin, the experimental yield corrected for background according to the LEPTO simulations is obtained as

Table 1
Four-dimensional grid used for the calculation of the acceptance. The full width of the respective dimension is given in the bottom row of the table.

ϕ/rad	$\lvert t\rvert$/(GeV/c)^2	Q^2/(GeV/c)^2	ν/GeV
$-\pi$ – $\frac{-3\pi}{4}$	0.08 – 0.15	1 – 1.5	8.5 – 11.45
$\frac{-3\pi}{4}$ – $\frac{-\pi}{2}$	0.15 – 0.22	1.5 – 2.24	11.45 – 15.43
.	0.22 – 0.36	2.24 – 3.34	15.43 – 20.78
.	0.36 – 0.5	3.34 – 5	20.78 – 28
.	0.5 – 0.64		
$\frac{3\pi}{4}$ – π			
$\Delta\phi$/rad	$\Delta\lvert t\rvert$/(GeV/c)^2	ΔQ^2/(GeV/c)^2	$\Delta\nu$/GeV
2π	0.56	4	19.5

$$\mathcal{Y}^{\pm}_{klmn} = \sum_{i=1}^{N^{\pm,\Delta\Omega_{klmn}}_{\text{data}}} \frac{1}{\Gamma(Q_i^2, \nu_i, E_{\mu,i})} - f^{\pm} \sum_{i=1}^{N^{\pm,\Delta\Omega_{klmn}}_{\text{L}}} \frac{1}{\Gamma(Q_i^2, \nu_i, E_{\mu,i})}. \tag{13}$$

Here, $N^{\pm,\Delta\Omega_{klmn}}_{\text{data}}$ is the number of measured events and $N^{\pm,\Delta\Omega_{klmn}}_{\text{L}}$ the number of LEPTO events within the phase-space element $\Delta\Omega_{klmn}$. The second sum represents the LEPTO simulations that are appropriately normalised by the factor $f^{\pm}$, which was introduced in Sect. 4. Each event is weighted with the transverse virtual-photon flux $\Gamma(Q_i^2, \nu_i, E_{\mu,i})$ in order to obtain the virtual-photon yield from the measured yields for muon-proton interactions, and with the $\pi^0 \to \gamma\gamma$ branching ratio. Radiative corrections are not applied but taken into account as systematic uncertainty.

The spin-dependent virtual-photon proton cross sections measured with positively or negatively charged muons are determined in each of the $(\phi_k, \lvert t\rvert_l)$ bins as luminosity-normalised experimental yield averaged over the measured ranges $\Delta Q^2 = 4\,(\text{GeV}/c)^2$ and $\Delta\nu = 19.5\,\text{GeV}$ as

$$\left\langle \frac{\mathrm{d}^2\sigma}{\mathrm{d}|t|\mathrm{d}\phi} \right\rangle^{\pm}_{\Delta\Omega_{kl}} = \frac{1}{\mathcal{L}^{\pm}\Delta\Omega_{kl}} \sum_{mn} \frac{\mathcal{Y}^{\pm}_{klmn}}{a(\Delta\Omega_{klmn})}. \tag{14}$$

Here, $\Delta\Omega_{kl} = \Delta\phi_k \Delta|t|_l \Delta Q^2 \Delta\nu$, $\mathcal{L}^{\pm}$ denotes the luminosity and $a(\Delta\Omega_{klmn})$ the acceptance in the phase-space element $\Delta\Omega_{klmn}$.

The spin-independent virtual-photon proton cross section is obtained according to Eq. (3) as the average of the two spin-dependent cross sections given in Eq. (14):

$$\left\langle \frac{\mathrm{d}^2\sigma}{\mathrm{d}|t|\mathrm{d}\phi} \right\rangle_{\Delta\Omega_{kl}} = \frac{1}{2}\left(\left\langle \frac{\mathrm{d}^2\sigma}{\mathrm{d}|t|\mathrm{d}\phi} \right\rangle^{+}_{\Delta\Omega_{kl}} + \left\langle \frac{\mathrm{d}^2\sigma}{\mathrm{d}|t|\mathrm{d}\phi} \right\rangle^{-}_{\Delta\Omega_{kl}} \right). \tag{15}$$

The cross section integrated over the full 2π-range in ϕ is obtained as

$$\left\langle \frac{\mathrm{d}\sigma}{\mathrm{d}|t|} \right\rangle_{\Delta\Omega_l} = \sum_k \Delta\phi_k \left\langle \frac{\mathrm{d}^2\sigma}{\mathrm{d}|t|\mathrm{d}\phi} \right\rangle_{\Delta\Omega_{kl}}, \tag{16}$$

with $\Delta\Omega_l = \Delta|t|_l \Delta Q^2 \Delta\nu$. Similarly, the $|t|$-averaged cross section in the measured range is given by

$$\left\langle \frac{\mathrm{d}^2\sigma}{\mathrm{d}|t|\mathrm{d}\phi} \right\rangle_{\Delta\Omega_k} = \frac{1}{\Delta|t|} \sum_l \Delta|t|_l \left\langle \frac{\mathrm{d}^2\sigma}{\mathrm{d}|t|\mathrm{d}\phi} \right\rangle_{\Delta\Omega_{kl}}, \tag{17}$$

with $\Delta\Omega_k = \Delta\phi_k \Delta|t| \Delta Q^2 \Delta\nu$.

The systematic uncertainties on the extracted values of the cross section are shown in Table 2, arranged in four groups. The first group contains the systematic uncertainties from the determination of the integrated beam flux. The second group contains possible systematic effects studied by the Monte Carlo simulation, which are related to the uncertainty on the energy thresholds for the detection of the low-energetic photon in the electromagnetic calorimeters, and the uncertainty on the determination of the acceptance. The third group contains the systematic uncertainties related to a variation of the energy and momentum balance of the kinematic fit, the influence of background originating from the production of ω mesons and the estimated influence of radiative corrections including the possible impact of a ϕ modulation [28,29]. The largest systematic effects appear in the fourth group, which contains two elements: (i) the uncertainty related to the estimation of non-exclusive background as described in Sect. 4; (ii) the uncertainty due to an observed mismatch between the measured single-photon yield in the 2012 COMPASS data and the corresponding Monte Carlo simulation of the Bethe-Heitler process. It appears in a kinematic region where single-photon production is dominated by the Bethe-Heitler cross section, and it is related to different intensities of positive and negative muon beams for the data analysed in this paper. The mismatch is discussed in Refs. [21,30]. The total systematic uncertainty Σ is obtained by quadratic summation of its components for each bin separately.

Table 2
Summary of the estimated relative systematic uncertainties for the $|t|$ and ϕ-dependent cross sections and the integrated cross section. The values are given in percent. Note that the uni-directional uncertainty $\sigma_{\uparrow}$ is a positive number, and $\sigma_{\downarrow}$ is a negative number.

Source	$\sigma^t_{\uparrow}$	$-\sigma^t_{\downarrow}$	$\sigma^{\phi}_{\uparrow}$	$-\sigma^{\phi}_{\downarrow}$	$\sigma_{\uparrow}$	$-\sigma_{\downarrow}$
μ^+ flux	2	2	2	2	2	2
μ^- flux	2	2	2	2	2	2
ECAL threshold	5	5	5	5	5	5
acceptance	4	7	4	7	4	7
kinem. fit	0	7	0	7	0	7
ω background	0	1	0	1	0	1
rad. corr.	2	5	2	5	2	5
LEPTO norm.	5–28	3–11	5–51	3–21	8	3
yield mismatch	4–13	3–7	0–12	3–12	9	5
$\sum$	12–29	13–18	12–53	13–25	14	14

6. Results

For the background corrected final data sample the average kinematics are $\langle Q^2\rangle = 2.0\,(\text{GeV}/c)^2$, $\langle\nu\rangle = 12.8\,\text{GeV}$, $\langle x_{Bj}\rangle = 0.093$ and $\langle -t\rangle = 0.256\,(\text{GeV}/c)^2$. The dependences of the measured cross section on $|t|$ and ϕ are shown in Fig. 6, with the numerical values given in Table 3. The cross section in bins of $|t|$ is shown in the top panel of Fig. 6. It appears to be consistent with an exponential decrease with increasing $|t|$ for values of $|t|$ larger than about $0.25\,(\text{GeV}/c)^2$, while at smaller $|t|$ the t-dependence becomes weaker. Our result is compared to the predictions of two versions of the Goloskokov-Kroll (GK) model [15,31]. The results of the GK model shown in this letter are obtained by integrating over the analysis range in the same way as it is done for the data. The dashed-dotted curve represents the cross section from the earlier version [15] as a function of $|t|$, while the upwards pointing triangles correspond to the cross section averaged over $|t|$ bins of the data. The mean cross sections for the full t-range are compared in the rightmost part of this panel. Analogously, the dotted curve and the downward pointing triangles correspond to the later version of the model [31], which was inspired by the results presented in this Letter. We observe that for the earlier version of the model the magnitude of the predicted cross section overshoots our measurement by approximately a factor of two.

The cross section as a function of ϕ averaged over the full measured t-range is shown in the bottom panel of Fig. 6 in eight ϕ

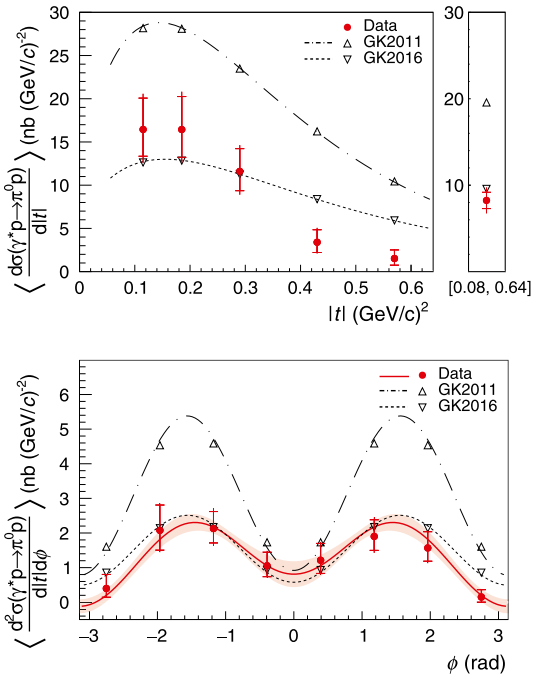

Fig. 6. Average value of the differential virtual-photon proton cross section $\langle \frac{d\sigma}{d|t|} \rangle$ as a function of $|t|$ (top) and $\langle \frac{d^2\sigma}{d|t|d\phi} \rangle$ as a function of ϕ (bottom). For the top panel the data was integrated over ϕ, while for the bottom panel it was averaged over the range $0.08\,(\mathrm{GeV}/c)^2 < |t| < 0.64\,(\mathrm{GeV}/c)^2$. The result of an integration over ϕ and $|t|$ is shown in the right-most part of the top panel. Inner error bars indicate the statistical uncertainty, outer error bars the quadratic sum of statistical and systematic uncertainties. The data is compared with two predictions of the GK model [15,31]. Radiative corrections are not applied but an estimate is included in the systematic uncertainties.

Table 3
Numerical values of the average cross sections shown in Fig. 6. For details see caption of Fig. 6.

Lower ϕ bin limit	$\left\langle \frac{d^2\sigma}{d\|t\|d\phi} \right\rangle / \frac{\mathrm{nb}}{(\mathrm{GeV}/c)^2}$	Lower $\|t\|$ bin limit	$\left\langle \frac{d\sigma}{d\|t\|} \right\rangle / \frac{\mathrm{nb}}{(\mathrm{GeV}/c)^2}$
$-\pi$	$0.4\,^{+\,0.4}_{-\,0.3}\|_{\mathrm{stat}}\,^{+\,0.1}_{-\,0.1}\|_{\mathrm{sys}}$	0.08	$16.4\,^{+\,3.6}_{-\,3.1}\|_{\mathrm{stat}}\,^{+\,2.0}_{-\,2.3}\|_{\mathrm{sys}}$
$\frac{-3\pi}{4}$	$2.1\,^{+\,0.7}_{-\,0.6}\|_{\mathrm{stat}}\,^{+\,0.3}_{-\,0.3}\|_{\mathrm{sys}}$	0.15	$16.4\,^{+\,3.8}_{-\,3.2}\|_{\mathrm{stat}}\,^{+\,2.1}_{-\,2.1}\|_{\mathrm{sys}}$
$\frac{-\pi}{2}$	$2.1\,^{+\,0.5}_{-\,0.4}\|_{\mathrm{stat}}\,^{+\,0.3}_{-\,0.3}\|_{\mathrm{sys}}$	0.22	$11.6\,^{+\,2.6}_{-\,2.2}\|_{\mathrm{stat}}\,^{+\,1.5}_{-\,1.5}\|_{\mathrm{sys}}$
$\frac{-\pi}{4}$	$1.1\,^{+\,0.4}_{-\,0.3}\|_{\mathrm{stat}}\,^{+\,0.2}_{-\,0.1}\|_{\mathrm{sys}}$	0.36	$3.4\,^{+\,1.4}_{-\,1.2}\|_{\mathrm{stat}}\,^{+\,0.8}_{-\,0.5}\|_{\mathrm{sys}}$
0	$1.2\,^{+\,0.5}_{-\,0.4}\|_{\mathrm{stat}}\,^{+\,0.2}_{-\,0.2}\|_{\mathrm{sys}}$	0.5	$1.5\,^{+\,1.0}_{-\,0.8}\|_{\mathrm{stat}}\,^{+\,0.4}_{-\,0.3}\|_{\mathrm{sys}}$
$\frac{\pi}{4}$	$1.9\,^{+\,0.5}_{-\,0.4}\|_{\mathrm{stat}}\,^{+\,0.3}_{-\,0.2}\|_{\mathrm{sys}}$		
$\frac{\pi}{2}$	$1.6\,^{+\,0.5}_{-\,0.4}\|_{\mathrm{stat}}\,^{+\,0.2}_{-\,0.2}\|_{\mathrm{sys}}$		
$\frac{3\pi}{4}$	$0.2\,^{+\,0.2}_{-\,0.1}\|_{\mathrm{stat}}\,^{+\,0.1}_{-\,0.0}\|_{\mathrm{sys}}$		

bins of equal width. The full dots show the measured cross section for each bin and the solid curve represents the fit described below.

In order to extract the different contributions to the spin-independent cross section, a binned maximum-likelihood fit is applied to the data according to Eq. (4). In the fit, the measured average value of the virtual-photon polarisation parameter is used, $\epsilon = 0.996$. The ϕ-integrated cross section determined by the fit is obtained as

$$\left\langle \frac{d\sigma_T}{d|t|} + \epsilon \frac{d\sigma_L}{d|t|} \right\rangle = (8.2 \pm 0.9_{\mathrm{stat}}\,^{+\,1.2}_{-\,1.2}|_{\mathrm{sys}}) \frac{\mathrm{nb}}{(\mathrm{GeV}/c)^2}. \tag{18}$$

The TT and LT interference terms are obtained as

$$\left\langle \frac{d\sigma_{TT}}{d|t|} \right\rangle = (-6.1 \pm 1.3_{\mathrm{stat}}\,^{+\,0.7}_{-\,0.7}|_{\mathrm{sys}}) \frac{\mathrm{nb}}{(\mathrm{GeV}/c)^2} \tag{19}$$

and

$$\left\langle \frac{d\sigma_{LT}}{d|t|} \right\rangle = (1.5 \pm 0.5_{\mathrm{stat}}\,^{+\,0.3}_{-\,0.2}|_{\mathrm{sys}}) \frac{\mathrm{nb}}{(\mathrm{GeV}/c)^2}. \tag{20}$$

We observe a large negative contribution by σ_{TT} and a smaller positive one by σ_{LT}, which indicates a significant role of transversely polarised photons in exclusive π^0 production.

The ϕ-dependence of the measured cross section is compared to the calculations of the GK model in the bottom panel of Fig. 6. Apart from the discrepancy in the magnitude of cross sections mentioned before, here we observe also different shapes for the measurement and the model predictions, which indicates that the relative contributions of the interference terms σ_{TT} and σ_{LT} are different when comparing measurement and model.

According to Eqs. (5) to (8), the different terms contributing to the cross section for exclusive pseudoscalar meson production, which appear in Eq. (4), depend on GPDs $\tilde{H}$, $\tilde{E}$, H_T and $\overline{E}_T = 2\tilde{H}_T + E_T$. For π^0 production a large contribution from transversely polarised virtual photons is expected, which is mainly generated by the chiral-odd GPD $\overline{E}_T$. It manifests itself in a large contribution from σ_{TT} and a dip in the differential cross section $d\sigma/dt$ as $|t|$ decreases to zero. These features are in qualitative agreement with our results and also with earlier measurements at different kinematics [9,10,13]. The COMPASS results on exclusive π^0 production provide significant constraints on modelling the chiral-odd GPDs, in particular GPD $\overline{E}_T$.

7. Summary and conclusion

Using exclusive π^0 muoproduction we have measured the t-dependence of the virtual-photon proton cross section for hard exclusive π^0 production at $\langle Q^2 \rangle = 2.0\ (\mathrm{GeV}/c)^2$, $\langle \nu \rangle = 12.8$ GeV, $\langle x_{Bj} \rangle = 0.093$ and $\langle -t \rangle = 0.256\ (\mathrm{GeV}/c)^2$. Fitting the azimuthal dependence reveals a large negative contribution by σ_{TT} and a smaller positive one by σ_{LT}, which indicates a significant role of transversely polarised photons in exclusive π^0 production. These results provide important input for modelling Generalised Parton Distributions. In the context of the phenomenological GK model, the statistically significant TT contribution constitutes clear experimental evidence for the existence of the chiral-odd GPD $\overline{E}_T$.

Declaration of competing interest

The authors declare that they have no known competing financial interests or personal relationships that could have appeared to influence the work reported in this paper.

Acknowledgements

We thank Sergey Goloskokov and Peter Kroll for their continuous support with model predictions, Pierre Guichon for the evaluation of the Bethe-Heitler contribution taking into account the muon mass and Andrei Afanasev for the discussion on the radiative corrections. We gratefully acknowledge the support of the CERN management and staff and the skill and effort of the technicians of our collaborating institutes.

References

[1] D. Müller, D. Robaschik, B. Geyer, F.-M. Dittes, J. Hořejši, Fortschr. Phys. 42 (1994) 101.
[2] X.-D. Ji, Phys. Rev. Lett. 78 (1997) 610.
[3] X.-D. Ji, Phys. Rev. D 55 (1997) 7114.
[4] A.V. Radyushkin, Phys. Lett. B 380 (1996) 417.
[5] A.V. Radyushkin, Phys. Rev. D 56 (1997) 5524.
[6] J.C. Collins, L. Frankfurt, M. Strikman, Phys. Rev. D 56 (1997) 2982.
[7] A. Airapetian, et al., HERMES Collaboration, Phys. Lett. B 659 (2008) 486.
[8] R. de Masi, et al., CLAS Collaboration, Phys. Rev. C 77 (2008) 042201.
[9] I. Bedlinskiy, et al., CLAS Collaboration, Phys. Rev. Lett. 109 (2012) 112001.
[10] I. Bedlinskiy, et al., CLAS Collaboration, Phys. Rev. C 90 (2014) 025205.

[11] A. Kim, et al., CLAS Collaboration, Phys. Lett. B 768 (2017) 168.
[12] E. Fuchey, et al., Hall A Collaboration, Phys. Rev. C 83 (2011) 025201.
[13] M. Defurne, et al., Hall A Collaboration, Phys. Rev. Lett. 117 (2016) 262001.
[14] M. Mazouz, et al., Hall A Collaboration, Phys. Rev. Lett. 118 (2017) 222002.
[15] S.V. Goloskokov, P. Kroll, Eur. Phys. J. A 47 (2011) 112.
[16] S. Ahmad, G.R. Goldstein, S. Liuti, Phys. Rev. D 79 (2009) 054014.
[17] M. Göckeler, et al., Phys. Rev. Lett. 98 (2007) 222001.
[18] P. Abbon, et al., COMPASS Collaboration, Nucl. Instrum. Methods A 577 (2007) 455.
[19] P. Abbon, et al., COMPASS Collaboration, Nucl. Instrum. Methods A 779 (2015) 69.
[20] F. Gautheron, et al., COMPASS Collaboration, SPSC-P-340, CERN-SPSC-2010-014.
[21] P. Jörg, Deeply Virtual Compton Scattering at CERN - What is the Size of the Proton?, PhD thesis, University of Freiburg, 2018, https://doi.org/10.6094/UNIFR/12397;
P. Jörg, Exploring the Size of the Proton, Springer International Publishing, 2018, https://doi.org/10.1007/978-3-319-90290-6.
[22] R. Mount, Nucl. Instrum. Methods 187 (1981) 401.
[23] B. Adeva, et al., SMC Collaboration, Nucl. Instrum. Methods A 343 (1994) 363.
[24] T. Szameitat, New Geant4-based Monte Carlo Software for the COMPASS-II Experiment at CERN, PhD thesis, University of Freiburg, 2017, https://doi.org/10.6094/UNIFR/11686.
[25] C. Adolph, et al., COMPASS Collaboration, Phys. Lett. B 718 (2013) 922.
[26] A. Sandacz, P. Sznajder, HEPGEN – generator for hard exclusive leptoproduction, arXiv:1207.0333, 2012.
[27] C. Regali, Exclusive Event Generation for the COMPASS-II Experiment at CERN and Improvements for the Monte-Carlo Chain, PhD thesis, University of Freiburg, 2016, https://doi.org/10.6094/UNIFR/11449.
[28] M. Gorzellik, Cross-section Measurement of Exclusive π^0 Muoproduction and Firmware Design for an FPGA-based Detector Readout, PhD thesis, University of Freiburg, 2018, https://doi.org/10.6094/UNIFR/15945.
[29] A. Afanasev, I. Akushevich, V. Burkert, K. Joo, Phys. Rev. D 66 (2002) 074004.
[30] R. Akhunzyanov, et al., COMPASS Collaboration, Phys. Lett. B 793 (2019) 188.
[31] S.V. Goloskokov, P. Kroll, private communications, 2016.

The COMPASS Collaboration

M.G. Alexeev [y], G.D. Alexeev [g], A. Amoroso [y,z], V. Andrieux [i,ab], N.V. Anfimov [g], V. Anosov [g], A. Antoshkin [g], K. Augsten [g,r], W. Augustyniak [ac], C.D.R. Azevedo [a], B. Badełek [ad], F. Balestra [y,z], M. Ball [c], J. Barth [c], R. Beck [c], Y. Bedfer [t], J. Bernhard [l,i], M. Bodlak [q], P. Bordalo [k,1], F. Bradamante [w,x], A. Bressan [w,x], M. Büchele [h], V.E. Burtsev [aa], W.-C. Chang [u], C. Chatterjee [f], M. Chiosso [y,z], A.G. Chumakov [aa], S.-U. Chung [o,2,3], A. Cicuttin [x,4], M.L. Crespo [x,4], S. Dalla Torre [x], S.S. Dasgupta [f], S. Dasgupta [w,x], O.Yu. Denisov [z,*], L. Dhara [f], S.V. Donskov [s], N. Doshita [af], Ch. Dreisbach [o], W. Dünnweber [5], R.R. Dusaev [aa], A. Efremov [g], P.D. Eversheim [c], M. Faessler [5], A. Ferrero [t], M. Finger [q], M. Finger Jr. [q], H. Fischer [h], C. Franco [k], N. du Fresne von Hohenesche [l,i], J.M. Friedrich [o,*], V. Frolov [g,i], E. Fuchey [t], F. Gautheron [b,ab], O.P. Gavrichtchouk [g], S. Gerassimov [n,o], J. Giarra [l], I. Gnesi [y,z], M. Gorzellik [h,6], A. Grasso [y,z], A. Gridin [g], M. Grosse Perdekamp [ab], B. Grube [o], A. Guskov [g], D. Hahne [d], G. Hamar [x], D. von Harrach [l], R. Heitz [ab], F. Herrmann [h], N. Horikawa [p,7], N. d'Hose [t], C.-Y. Hsieh [u,8], S. Huber [o], S. Ishimoto [af,9], A. Ivanov [y,z], T. Iwata [af], M. Jandek [r], V. Jary [r], R. Joosten [c], P. Jörg [h,10], K. Juraskova [r], E. Kabuß [l], F. Kaspar [o], A. Kerbizi [w,x], B. Ketzer [c], G.V. Khaustov [s], Yu.A. Khokhlov [s,11], Yu. Kisselev [g], F. Klein [d], J.H. Koivuniemi [b,ab], V.N. Kolosov [s], K. Kondo Horikawa [af], I. Konorov [n,o], V.F. Konstantinov [s], A.M. Kotzinian [z,12], O.M. Kouznetsov [g], Z. Kral [q], M. Krämer [o], F. Krinner [o], Z.V. Kroumchtein [g,30], Y. Kulinich [ab], F. Kunne [t], K. Kurek [ac], R.P. Kurjata [ae], A. Kveton [r], S. Levorato [x], Y.-S. Lian [u,13], J. Lichtenstadt [v], P.-J. Lin [t,14], R. Longo [ab], V.E. Lyubovitskij [aa,15], A. Maggiora [z], A. Magnon [ab,29], N. Makins [ab], N. Makke [x,4], G.K. Mallot [i], S.A. Mamon [aa], B. Marianski [ac], A. Martin [w,x], J. Marzec [ae], J. Matoušek [w,x,q], T. Matsuda [m], G.V. Meshcheryakov [g], M. Meyer [ab,t], W. Meyer [b], Yu.V. Mikhailov [s], M. Mikhasenko [c], E. Mitrofanov [g], N. Mitrofanov [g], Y. Miyachi [af], A. Moretti [w,x], C. Naim [t], A. Nagaytsev [g], D. Neyret [t], J. Nový [r,i], W.-D. Nowak [l], G. Nukazuka [af], A.S. Nunes [k], A.G. Olshevsky [g], M. Ostrick [l], D. Panzieri [z,16], B. Parsamyan [y,z], S. Paul [o], J.-C. Peng [ab], F. Pereira [a], M. Pešek [q], D.V. Peshekhonov [g], M. Pešková [q], N. Pierre [l,t], S. Platchkov [t], J. Pochodzalla [l], V.A. Polyakov [s], J. Pretz [d,17], M. Quaresma [u], C. Quintans [k], S. Ramos [k,1], C. Regali [h], G. Reicherz [b], C. Riedl [ab], D.I. Ryabchikov [s,o], A. Rybnikov [g], A. Rychter [ae], V.D. Samoylenko [s], A. Sandacz [ac], S. Sarkar [f], I.A. Savin [g], G. Sbrizzai [w,x], H. Schmieden [d], A. Selyunin [g], L. Silva [k], L. Sinha [f], M. Slunecka [g], J. Smolik [g], A. Srnka [e], D. Steffen [i,o], M. Stolarski [k], O. Subrt [i,r], M. Sulc [j], H. Suzuki [af,7], A. Szabelski [w,x,ac], T. Szameitat [h,6], P. Sznajder [ac], S. Tessaro [x], F. Tessarotto [x], A. Thiel [c], J. Tomsa [q], F. Tosello [z], V. Tskhay [n], S. Uhl [o], B.I. Vasilishin [aa], A. Vauth [d,i], B.M. Veit [l,i], J. Veloso [a], A. Vidon [t], M. Virius [r], M. Wagner [c], S. Wallner [o], M. Wilfert [l], K. Zaremba [ae], P. Zavada [g], M. Zavertyaev [n], E. Zemlyanichkina [g], Y. Zhao [x], M. Ziembicki [ae]

[a] *University of Aveiro, I3N - Physics Department, 3810-193 Aveiro, Portugal*
[b] *Universität Bochum, Institut für Experimentalphysik, 44780 Bochum, Germany* [18,19]
[c] *Universität Bonn, Helmholtz-Institut für Strahlen- und Kernphysik, 53115 Bonn, Germany* [18]
[d] *Universität Bonn, Physikalisches Institut, 53115 Bonn, Germany* [18]
[e] *Institute of Scientific Instruments of the CAS, 61264 Brno, Czech Republic* [20]
[f] *Matrivani Institute of Experimental Research & Education, Calcutta-700 030, India* [21]
[g] *Joint Institute for Nuclear Research, 141980 Dubna, Moscow region, Russia*
[h] *Universität Freiburg, Physikalisches Institut, 79104 Freiburg, Germany* [18,19]
[i] *CERN, 1211 Geneva 23, Switzerland*
[j] *Technical University in Liberec, 46117 Liberec, Czech Republic* [20]
[k] *LIP, 1649-003 Lisbon, Portugal* [22]

[l] Universität Mainz, Institut für Kernphysik, 55099 Mainz, Germany [18]
[m] University of Miyazaki, Miyazaki 889-2192, Japan [23]
[n] Lebedev Physical Institute, 119991 Moscow, Russia
[o] Technische Universität München, Physik Dept., 85748 Garching, Germany [18,5]
[p] Nagoya University, 464 Nagoya, Japan [23]
[q] Charles University in Prague, Faculty of Mathematics and Physics, 12116 Prague, Czech Republic [20]
[r] Czech Technical University in Prague, 16636 Prague, Czech Republic [20]
[s] State Scientific Center Institute for High Energy Physics of National Research Center 'Kurchatov Institute', 142281 Protvino, Russia
[t] IRFU, CEA, Université Paris-Saclay, 91191 Gif-sur-Yvette, France [19]
[u] Academia Sinica, Institute of Physics, Taipei 11529, Taiwan [24]
[v] Tel Aviv University, School of Physics and Astronomy, 69978 Tel Aviv, Israel [25]
[w] University of Trieste, Dept. of Physics, 34127 Trieste, Italy
[x] Trieste Section of INFN, 34127 Trieste, Italy
[y] University of Turin, Dept. of Physics, 10125 Turin, Italy
[z] Torino Section of INFN, 10125 Turin, Italy
[aa] Tomsk Polytechnic University, 634050 Tomsk, Russia [26]
[ab] University of Illinois at Urbana-Champaign, Dept. of Physics, Urbana, IL 61801-3080, USA [27]
[ac] National Centre for Nuclear Research, 00-681 Warsaw, Poland [28]
[ad] University of Warsaw, Faculty of Physics, 02-093 Warsaw, Poland [28]
[ae] Warsaw University of Technology, Institute of Radioelectronics, 00-665 Warsaw, Poland [28]
[af] Yamagata University, Yamagata 992-8510, Japan [23]

* Corresponding authors.
E-mail addresses: oleg.denisov@cern.ch (O.Yu. Denisov), jan.friedrich@cern.ch (J.M. Friedrich).

[1] Also at Instituto Superior Técnico, Universidade de Lisboa, Lisbon, Portugal.
[2] Also at Dept. of Physics, Pusan National University, Busan 609-735, Republic of Korea.
[3] Also at Physics Dept., Brookhaven National Laboratory, Upton, NY 11973, USA.
[4] Also at Abdus Salam ICTP, 34151 Trieste, Italy.
[5] Supported by the DFG cluster of excellence 'Origin and Structure of the Universe' (www.universe-cluster.de) (Germany).
[6] Supported by the DFG Research Training Group Programmes 1102 and 2044 (Germany).
[7] Also at Chubu University, Kasugai, Aichi 487-8501, Japan.
[8] Also at Dept. of Physics, National Central University, 300 Jhongda Road, Jhongli 32001, Taiwan.
[9] Also at KEK, 1-1 Oho, Tsukuba, Ibaraki 305-0801, Japan.
[10] Present address: Universität Bonn, Physikalisches Institut, 53115 Bonn, Germany.
[11] Also at Moscow Institute of Physics and Technology, Moscow Region, 141700, Russia.
[12] Also at Yerevan Physics Institute, Alikhanian Br. Street, Yerevan, 0036, Armenia.
[13] Also at Dept. of Physics, National Kaohsiung Normal University, Kaohsiung County 824, Taiwan.
[14] Supported by the P2IO LabEx Grant No. ANR-10-LABX-0038, Agence Nationale de la Recherche, France.
[15] Also at Institut für Theoretische Physik, Universität Tübingen, 72076 Tübingen, Germany.
[16] Also at University of Eastern Piedmont, 15100 Alessandria, Italy.
[17] Present address: RWTH Aachen University, III. Physikalisches Institut, 52056 Aachen, Germany.
[18] Supported by BMBF - Bundesministerium für Bildung und Forschung (Germany).
[19] Supported by FP7, HadronPhysics3, Grant 283286 (European Union).
[20] Supported by MEYS, Grant LM20150581 (Czech Republic).
[21] Supported by B.Sen fund (India).
[22] Supported by FCT, COMPETE and QREN, Grants CERN/FP 116376/2010, 123600/2011 and CERN/FIS-NUC/0017/2015 (Portugal).
[23] Supported by MEXT and JSPS, Grants 18002006, 20540299, 18540281 and 26247032, the Daiko and Yamada Foundations (Japan).
[24] Supported by the Ministry of Science and Technology, Taiwan.
[25] Supported by the Israel Academy of Sciences and Humanities (Israel).
[26] Supported by the Russian Federation program "Nauka" (Contract No. 0.1764.GZB.2017) (Russia).
[27] Supported by the National Science Foundation, Grant no. PHY-1506416 (USA).
[28] Supported by NCN, Grant 2017/26/M/ST2/00498 (Poland).
[29] Retired.
[30] Deceased.